



Strength and Failure Behaviors of a Jointed Rock Mass Anchored by Steel Bolts: A Numerical Modeling Study

Hong-Wen Jing · Xu-Xu Yang · Mao-Lin Zhang

Received: 11 November 2021 / Accepted: 12 August 2022 / Published online: 21 August 2022
© The Author(s), under exclusive licence to Springer Nature Switzerland AG 2022

Abstract Large deformation of anchored rock masses or pull-out failure of anchor bolts often occurs in tunneling practices. The existence of incipient joints in rock masses might account for the failure of anchor bolts. The strength of the anchored rock mass varied with the geometric property of the joints and might be less than the target value. A series of numerical modeling experiments have been carried out in the present study by utilizing the FLAC^{3D} software package. A novel method has been proposed to establish and validate numerical models such that they can simulate and extend physical experimental results. Accordingly, we demonstrated that the application of anchor bolts increases the strength of the jointed rock blocks but significantly depends on the orientation of incipient joints. The anchor bolt reduces the nonuniformity of the stress distribution, and the uniformity increases gradually with increasing bolt density. Moreover, the application of anchor bolts would keep the rock blocks as intact to contain the tendentious failure along the incipient joint planes. The findings

in the present study would benefit the stabilization of rock masses adjacent to an underground tunnel, especially at the initial stage of failure when only incipient joints exist.

Keywords Failure behavior · Anchored bolts · Incipient joints · FLAC^{3D} · Rock blocks

1 Introduction

After an underground tunnel was excavated, the redistribution of in situ stress and the heterogeneity of rock materials would bring out incipient joints in the rock mass. The incipient joints occur in the initial stage of fracturing and thus generally show a nonpersistent nature, which means that the joints are not fully connected with each other but interspaced by intact rock bridges. In rock engineering practices, incipient joints often develop over geological time or under construction disturbances into persistent ones (Hencher 2014), as long as there are no measures applied to treat them. For example, Lajtai et al. (1994) reported an observation of incipient joints in yield pillars of the potash mines of Saskatchewan. They characterized the joints into two typical patterns, which were the en echelon tensile crack array and the en echelon shear crack array. With increasing stress concentration, the shear crack array further collapsed, forming the envelope or hourglass structures of the rock pillars. Through in situ borehole camera monitoring, Li et al. (2012)

H.-W. Jing · M.-L. Zhang
State Key Laboratory for Geomechanics and Deep
Underground Engineering, China University of Mining
and Technology, Xuzhou 221116, China

X.-X. Yang (✉)
Shandong Key Laboratory of Civil Engineering Disaster
Prevention and Mitigation, Shandong University
of Science and Technology, Qingdao 266590, China
e-mail: yangxu@sust.edu.cn

also observed the occurrence of incipient joints in deeply buried tunnels of the Jinping II hydropower station. With the convergence of the surrounding rock mass, the incipient joints connected with each other by forming a macro failure plane in a tendentious path. Therefore, it is of great significance to fully understand the strength and failure behaviors of incipiently jointed rock blocks for the purpose of stabilizing underground tunnels (Sun et al. 2019; Yang et al. 2015).

Numerous studies have been implemented to examine the mechanical behaviors of rock blocks with incipient joints through either physical modeling or numerical modeling. With respect to the loading condition, these modeling studies were carried out under uniaxial compression (Cao et al. 2020; Yang et al. 2017), biaxial compression (Han et al. 2018), compressed shearing (Cao et al. 2018) or direct shearing conditions (Yang and Qiao 2018; Yang and Kulatilake 2019). Even though the abovementioned loading paths were different from those experienced by a rock block adjacent to an underground tunnel, the research shed light on the failure behaviors of incipiently jointed rock masses. A common conclusion obtained from these studies was that the failure mechanism of the incipiently jointed rock mass is always tendentious along a limited pathway that is significantly dependent on the joint orientation and the loading condition (Wong and Chau 1998; Wong et al. 2001). To contain the tendentious failure, the anchored bolt material seems to be capable of supporting these rock masses, for which stiff steel bars are inserted into them after all.

However, in underground tunnels with high in situ stress, improper setup of anchor bolts often results in them being pulled out or failing in the rock mass. Even with a high anchoring density (bolt number per unit area), the surrounding rock masses adjacent to underground tunnels still undergo large deformation failure through the development and coalescence of incipient joints (Jing et al. 2014). Thus, an understanding of the way in which these bolts work is essential to arrive at an optimal, safe and economic use (Grasselli 2005). Because of the significant effect of joints on rock mass stability, most researchers have attempted to determine how anchor bolts perform efficiently to resist shearing along joint surfaces. For example, Haas (1998) reported a laboratory study on limestone and schist blocks with resin-anchored bolts

at various angles. It was concluded that inclined bolts were stiffer and contributed more to the shear strength of the bolted joints than perpendicular ones. Pellet and Egger (1996) introduced an analytical model for predicting the role of bolts on the shear strength of rock joints. The interaction of the axial and shear forces mobilized in the bolts as well as the large plastic displacements of the bolt during the loading process was considered in the model. Indraratna et al. (2001) claimed that even for joints containing clay infill, the bolts contributed to increasing the strength and stiffness of the joint composite but were dependent on the normal stress levels and infill thickness. Recently, Wang et al. (2018) carried out a study on the shear behavior and acoustic emission characteristics of bolted rock joints with different roughness. In accordance with their research results, they suggested that the bolt elongation as well as the joint roughness would influence the shear strength of the bolted joints.

The above studies enhance our understanding of the support effect of anchor bolts on persistent joints, while little attention has been given to the problem of whether they are capable of supporting rock masses with incipient joints. After all, the final failure plane was not known in advance in incipiently jointed rock masses. In an incipiently jointed rock mass, the anchor bolts not only interact with the joints but also interact with the intact rock bridges. As a pioneer, Li et al. (2006) took the complicated system as a subject of study and investigated the constitutive model and damage mechanism of bolted rock masses containing incipient joints under compression-shearing and tension-shearing conditions. Our recent studies (Jing et al. 2014; Meng et al. 2013) showed that the anchoring strength of a rock mass with joints was greater than that of a jointed rock mass without any bolts but was dependent on joint orientation. However, under more complicated stress conditions experienced by a rock block adjacent to an underground tunnel, the support effect of anchor bolts has not yet been completed and requires much more research effort.

Given the abovementioned problems, a series of numerical modeling experiments have been carried out in the present study to examine the support effect of anchor bolts on rock blocks that have incipient joints. The setup of the numerical models strictly followed the physical experiments conducted in a laboratory and was validated by the experimental results.

The establishment procedure is presented in detail in Sect. 2, and a method developed to create incipient joints in FLAC^{3D} models is introduced. By conducting confined compression tests on these numerical models, the results were displayed and analyzed in Sect. 3 in terms of stress distribution and shear deformation, and the support effects of anchor bolts were discussed. In Sect. 4, the strength behavior of the bolted rock mass is analyzed in detail. Based on the results, we achieved a better understanding of the support effect of anchor bolts from the sights of how they increase the strength of the entirety and contain the tendentious failure of the incipient joints planes. The findings would be beneficial for stabilizing rock masses adjacent to an underground tunnel, especially at the incipient stage of fracturing.

2 Setup and Validation of Numerical Models

2.1 Physical Experiment Setup

A large-scale experimental system was designed to explore the support effect of anchor bolts on jointed rock blocks with incipient joints. A bolted rock block model of 2.5 m × 2.5 m × 2.4 m was assumed to be separated from the wall of an underground tunnel in a coal mine, as shown in Fig. 1. For this bolted rock block, the major principal stress, σ_1 , acts in the vertical direction. The intermediate principal stress, σ_2 , acts in the lateral direction perpendicular to the rock mass shown in Fig. 1. The minor principal stress, σ_3 , acts in the lateral direction

perpendicular to the free surface. The free surface is used to apply anchor bolts to the rock mass. However, the rock block face opposite to the free surface along the σ_3 direction is assumed to be fixed due to the relatively small displacement in the surrounding rock mass of 2.5 m depth. To facilitate the physical modeling, the size of the synthetic jointed rock block used in the experiments was 0.5 m × 0.5 m × 0.48 m (see Fig. 2) to simulate the separated rock mass of size 2.5 m × 2.5 m × 2.4 m in Fig. 1. For more details about the similarity ratios used and applied boundary conditions, the reader is referred to our previous study (Jing et al. 2014; Zhang 2013). Moreover, a specially designed

Fig. 1 A bolted rock block containing incipient joints

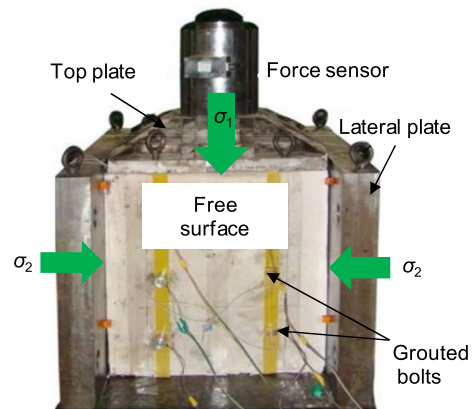
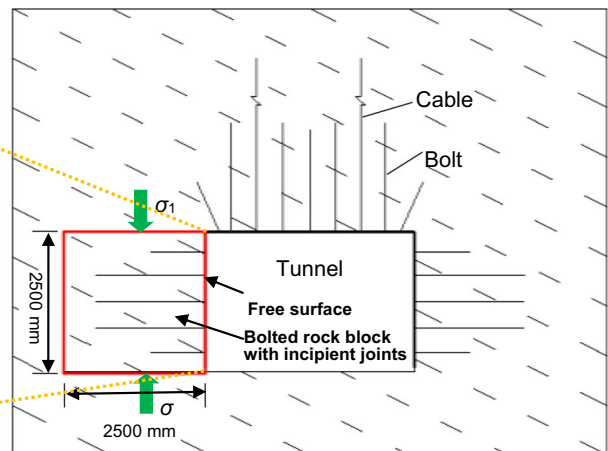
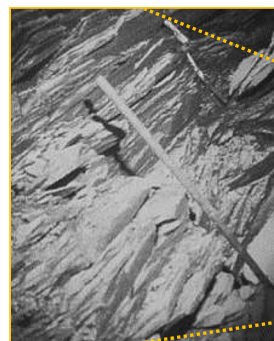


Fig. 2 Synthetic rock block model utilized in physical experiments

loading frame was used to apply the stress system on the synthetic jointed rock block, as shown in Fig. 2.

Mixing of C42.5 cement, plaster, 200 M silica flour and water in a mass ratio of 7:3:5:2.5 was adopted to fabricate the synthetic rock blocks. The mechanical properties of the synthetic rock-like materials were obtained through uniaxial compression tests, triaxial compression tests and indirect tension tests, and the corresponding results are listed in Table 1. In addition, to mimic nonpersistent incipient joints of, nine individual steel plates of 2 mm thickness and 100 mm length were inserted into the synthetic rock blocks to create joints when pouring the synthetic model material mixture. The individual joints were arranged in an en echelon and a symmetrical pattern, as shown in Fig. 3. Note that the images in Fig. 3 show a cross-section view of the joint configuration along the σ_2 direction, as indicated in Fig. 2, which means that the created joints penetrate the rock blocks along this direction. In the physical experiments, different joint orientations, such as $\alpha = 30^\circ$, 45° and 60° , were considered to verify their effects on the mechanical behaviors of the jointed rock blocks. Furthermore, to simulate the anchor bolt combo, an aluminum bar with a diameter of 3 mm and an anti-resistance glass fiber board with a thickness of 3 mm and an area of

$30 \times 30 \text{ mm}^2$ were chosen as the operating bolt and pallet, respectively. To investigate the effect of the number of bolts on the mechanical performance of the bolted rock block, 0, 3, 6 and 9 bolts were applied to the jointed rock blocks. Given that three different joint orientations were examined, a 3×4 test scenario matrix was considered in the present study.

The prepared specimens mentioned above were then subjected to compression tests using a TYS-500 testing machine, and the axial load, axial displacement and horizontal displacements were collected using a data acquisition system. The data obtained from the physical experiments were utilized to calibrate and validate a numerical model developed on the same synthetic bolted rock blocks using the FLAC^{3D} software package.

2.2 Numerical Model Setup

2.2.1 Mesh Model

To establish the numerical models by utilizing the FLAC^{3D} software package, the key procedure is to create individual nonpersistent joints. As shown in Fig. 3, the rock block models of the study model contain nine incipient joints arranged in an en echelon. To create individual joints and

Table 1 Mechanical properties of rock-like materials used in physical experiments

Properties	Densit (kg/m^3)	Young's modulus (GPa)	UCS (MPa)	Tensile strength (MPa)	Cohesion (kPa)	Friction angle (deg)
Values	16.35	0.44	3.77	0.51	58.3	35.26

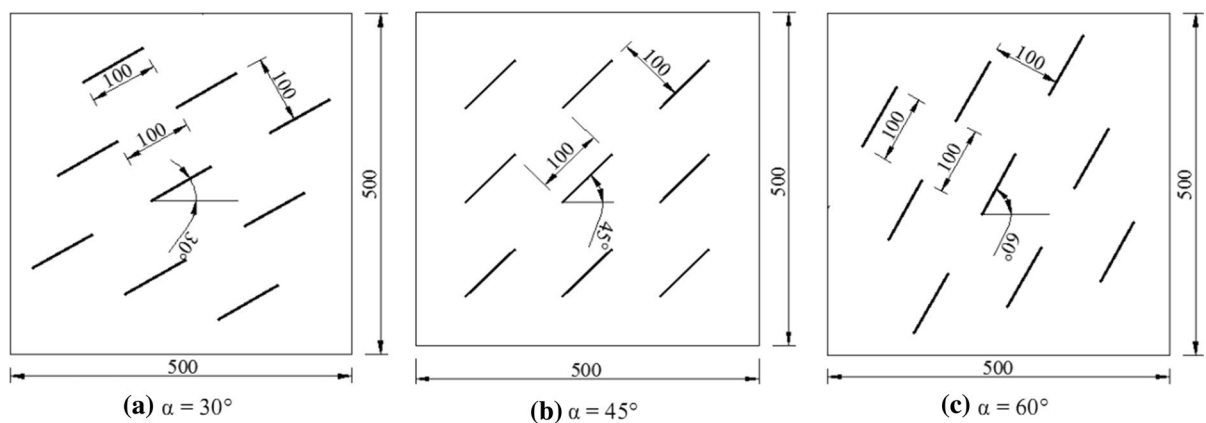


Fig. 3 Joint setup (unit: mm)

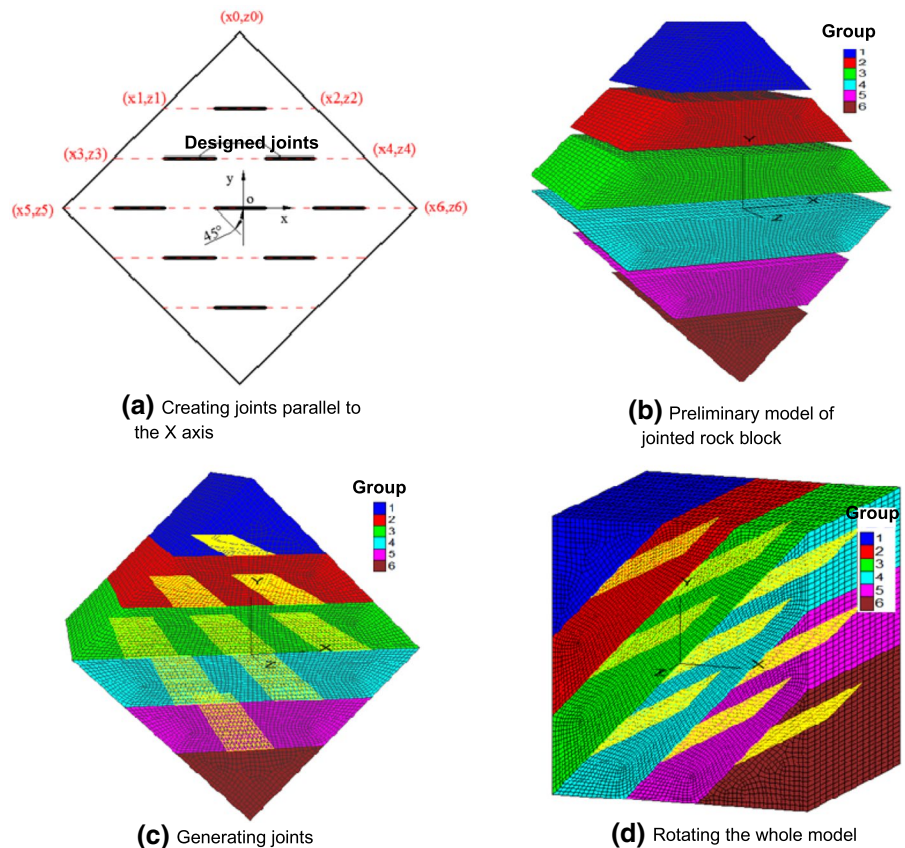
vary their orientations, a novel method was developed in the present study. In FLAC^{3D}, all the geometrical values, such as displacement and coordinates, are dependent on the node of the model, while property values, such as stress and quality, rely on the unit body, which is defined through the six or eight nodes around it. Therefore, as long as the node coordinates change, the geometric values will change, while the property values will not change. Accordingly, the joint surfaces were able to be added horizontally through coordinate rotation. After the contact surface of the joint was applied, a model rotation function was written in FISH language to obtain the required model with differently oriented joints. Specifically, the establishment of a mesh model with incipient joints is given as follows (see Fig. 4):

1. Establish a block geometric model rotating to a specific degree; see Fig. 4a;
2. Divide the block geometric model into geometric block combination models required for a simula-

- tion according to the vertical spacing of joints, as shown in Fig. 4b;
3. Mesh the geometric block combination models using the hexahedron element in the ANSYS software package;
4. Import the mesh model provided by ANSYS into FLAC^{3D} and use the command "generate separate" to separate the parts in the block combination mesh models and moving them to keep a certain distance from each other;
5. Generate interfaces with the side length being the joint length at the specified position on the surface of each grouped mesh, as shown in Fig. 4c;
6. Move the separated parts of the mesh model to contact each other, and use the "generate merge" command to merge the parts with the same coordinates outside the coverage area of interfaces, as shown in Fig. 4d.

The generated jointed rock model has a total of 95,040 units and 104,704 nodes. By utilizing the above procedure, the joint dip angle in the numerical

Fig. 4 Generating procedure of jointed rock model with dip angle of 45°



models was varied from 0° to 90° with an interval of 15°, i.e., $\alpha=0^\circ, 15^\circ, 30^\circ, 45^\circ, 60^\circ, 75^\circ$ and 90° . Thus, seven differently oriented rock block models containing incipient joints were generated to extend the physical experiments.

2.2.2 Mechanical Model, Parameters and Initial Conditions

After completing the structural design of the numerical models, the following is to constitute them to behave in a mechanical manner similar to the rock-like materials used in physical experiments. In view of the fact that the anchor bolts support the rock mass not only in the before-failure stage but also in the after-failure stage, a strain-softening constitutive model was chosen to control their mechanical behaviors. Compared with other constitutive models, the strain-softening constitutive model can well derive the postpeak failure characteristics of a rock mass by defining the relationship of cohesive strength and internal friction angle with the increment of plastic principal strain after the plastic yield starts. It includes a shear strength yield criterion given by:

$$f_s = [(\sigma_3 - \sigma_1)/2] - [c \cdot \cos \phi - 0.5(\sigma_1 + \sigma_3) \sin \phi] \tag{1}$$

in which σ_1 and σ_3 imply the principal stresses applied on model materials, and c and ϕ imply the cohesive strength and internal friction angle.

In FLAC^{3D}, the strain-softening constitutive model also includes a strength yield criterion under tensile stress, which is given by:

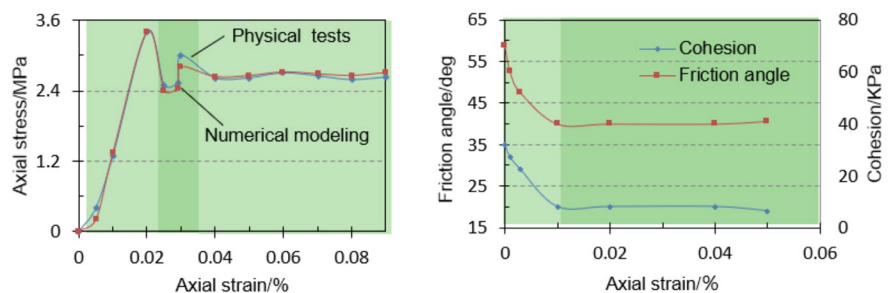
$$f_t = \sigma_t - \sigma_3 \tag{2}$$

where σ_t implies the tensile stress applied on the model materials.

The values of the prepeak material parameters used for the numerical models were the same as those used for the physical experiments, as shown in Table 1. The postpeak strain-softening parameters, such as cohesive strength and internal friction angle, were obtained by calibrating the stress–strain curves of multi-jointed rock models with a dip angle of 45° under uniaxial compression tests. Figure 5 displays the calibrating process through an inversion study. As shown in Fig. 5a, the stress–strain curve obtained from physical tests was first given, and the stress–strain curve obtained through numerical modeling was attempted to coincide it by constantly modifying the friction angle and cohesion parameters with increasing uniaxial strain values, as shown in Fig. 5b. The modification of the friction angle and cohesion was a trial–error process. Generally, we decreased the values of both parameters from those for prepeak material parameters, as listed in Table 1. With the increment of the uniaxial strain values, say when the uniaxial strain is 0.1, a combination of lower friction angle and cohesion values would derive a satisfactory postpeak behavior, as shown in Fig. 5a; then, there is no need to further decrease the values of both parameters. Accordingly, a series of friction angle and cohesion combination values were determined, as shown in Fig. 5b, and used for other numerical models.

The aforementioned mechanical parameters were applied to all the unit bodies in the numerical model to mimic intact rock materials. However, as if the unit bodies were located in the defined joint area, the values of the friction coefficient and cohesive strength for interfaces would be reset as zero, while the other mechanical parameters were kept unchanged to

Fig. 5 Calibration of post-peak strain-softening parameters



(a) Comparison of stress–strain curves between physical test and numerical simulation

(b) Calibrated post-peak strain-softening parameters

simulate open smooth joint surfaces, which is consistent with that in physical experiments.

Moreover, the anchor bolts were mimicked by utilizing the rock bolt structural element in the FLAC^{3D} package. The mechanical parameters used for the anchor bolts were the same as those used in the physical experiments. The values of the mechanical parameters for the anchor bolts are listed in Table 2. Furthermore, a preload of 3.0 kN was applied on each anchor bolt to provide the initial support stress, σ_3 . On the other hand, σ_2 was set to 1.0 MPa and applied from the lateral sides of the numerical model.

2.3 Validation of Numerical Models

To validate the reliability of numerical modeling, this section compares and analyzes the results of numerical modeling and physical experiments in the case of multi-jointed rock blocks with and without anchor bolts. In particular, Fig. 6 shows a comparison of the failure patterns of unbolted jointed rock blocks with a dip angle of 45°. In accordance with Fig. 6, for numerical modeling, plastic failure occurs in all rock bridges along the joint inclined plane, forming several large macroscopic failure planes, and the final failure pattern was consistent with the physical experiments. In addition, Fig. 7 also demonstrates the consistency of the stress–strain curves between the physical experiments and numerical modeling.

Moreover, Figs. 8 and 9 display the comparison of the test results of bolted jointed rock blocks with

Table 2 Mechanical parameter values for anchored bolts

Properties	Cross section area (mm ²)	Elastic modulus (GPa)	Yield force (kN)	Extensibility (%)
Values	7.065	35.0	20.0	≥ 16

Fig. 6 Comparison of failure pattern of jointed rock blocks with dip angle 45°

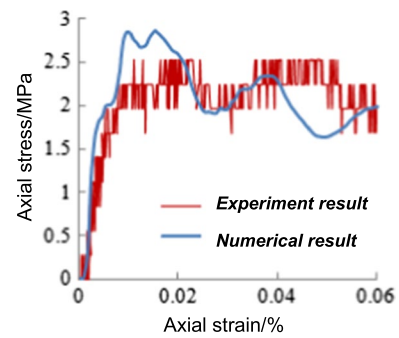
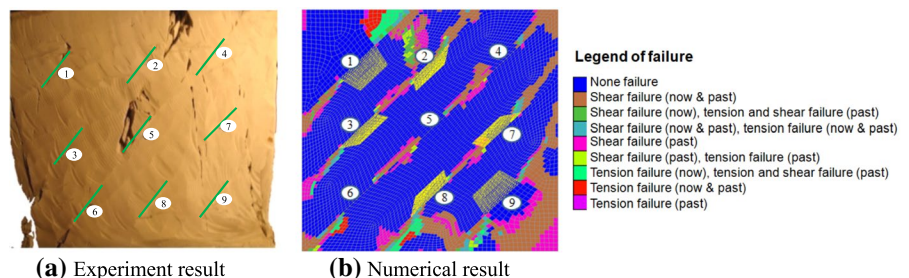


Fig. 7 Comparison of stress–strain curves of jointed rock blocks with dip angle 45°

a dip angle of 30°. In accordance with Fig. 8, we could find several similar local failure regions in the experimental and simulation models. Specifically, adjacent to the free surface both in the experimental and simulation models, the rock mass was significantly ruptured or deformed because of the coalescence of joints 1, 3 and 6. On the other side of the model, in the experimental model, joints 4, 7 and 9 were connected with each other by the cracks developed from the adjacent joint tips. In the numerical model, between joints 4, 7 and 9, there were shear and tension failures occurring to their adjacent joint tips. In Fig. 9, even though there were some deviations between the experimental and numerical curves, the peak stress and the postpeak stress showed a similar trend with each other. Based on the comparison between the numerical and experimental results we observed from Figs. 8 and 9, we conclude that the test results obtained through numerical modeling were similar to those obtained in physical experiments. Above all, the established numerical models were capable of deriving the mechanical behaviors obtained in physical experiments; thus, they were utilized to further explore the influences of joint orientation and the number of

Fig. 8 Comparison of failure pattern of jointed rock blocks with dip angle 30°

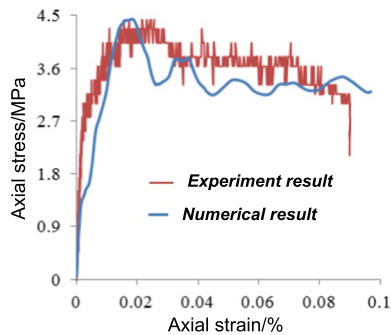
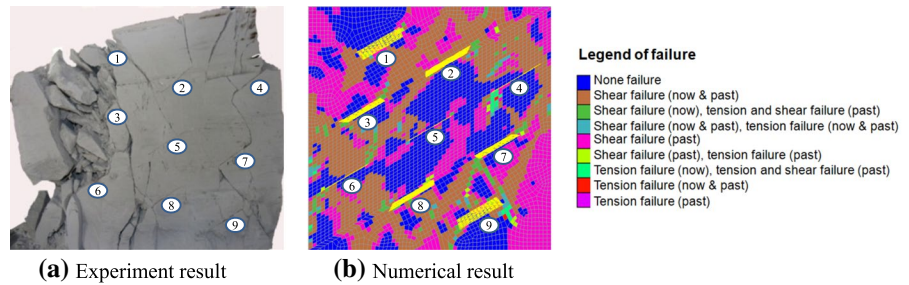


Fig. 9 Comparison of stress–strain curves of jointed rock blocks with dip angle 30°

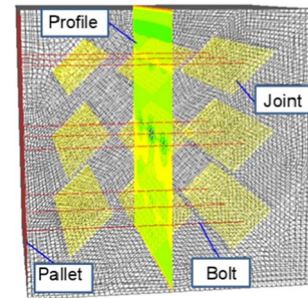


Fig. 10 Selected profile position in insides of jointed rock block

anchor bolts on the mechanical performance of rock blocks with incipient joints.

3 Results and Analysis

3.1 Influence of Anchor Bolts on Stress Distribution

In this section, by analyzing the stress state inside jointed rock blocks before and after the application of anchor bolts, the support effect of anchor bolts was studied. After the calculation of various numerical models was completed, a profile was selected along the middle of the model perpendicular to the bolts to draw the cloud map of the maximum principal stress distribution. The selected profile position is shown in Fig. 10. As an example, Fig. 11 displays the distribution of the maximum principal stress inside the jointed rock block of $\alpha=45^\circ$. Note that to facilitate the research, the number of rock bolts applied in jointed rock blocks was converted into the density of rock bolts per unit area in the actual project. Thus, the densities of 3, 6 and 9 rock bolts corresponded to 0.48, 0.96 and 1.44 m^{-2} , respectively.

As shown in Fig. 11, the application of the anchor bolt reduced the nonuniformity of the stress distribution in the jointed rock blocks, and the uniformity increased gradually with increasing bolt density. Note that the positive values imply tensile stress, while the negative values imply compression stress. In particular, due to the existence of joints, a tensile stress region appeared in the middle of the model, as shown in Fig. 11a. Under the "friction effect" at the end, the stress concentration of the rock mass near the upper and lower loading planes was relatively obvious. After the application of 3 bolts (i.e., $\rho=0.48 \text{ m}^{-2}$), the stress concentration zone and tensile stress zone of the rock block along the pallets disappeared, and the maximum principal stress showed a yellow compressive stress zone of 2.0 MPa. However, there was still a red tensile stress zone with a peak value of 2.0 MPa near the intermediate joints, as shown in Fig. 11b. With increasing bolt density, the maximum tensile stress of the joints decreased to 1.5 MPa when 6 bolts were applied, i.e., $\rho=0.96 \text{ m}^{-2}$. However, when 9 bolts were applied, the tensile stress disappeared, and the stress distribution was more uniform, as shown in Fig. 11d.

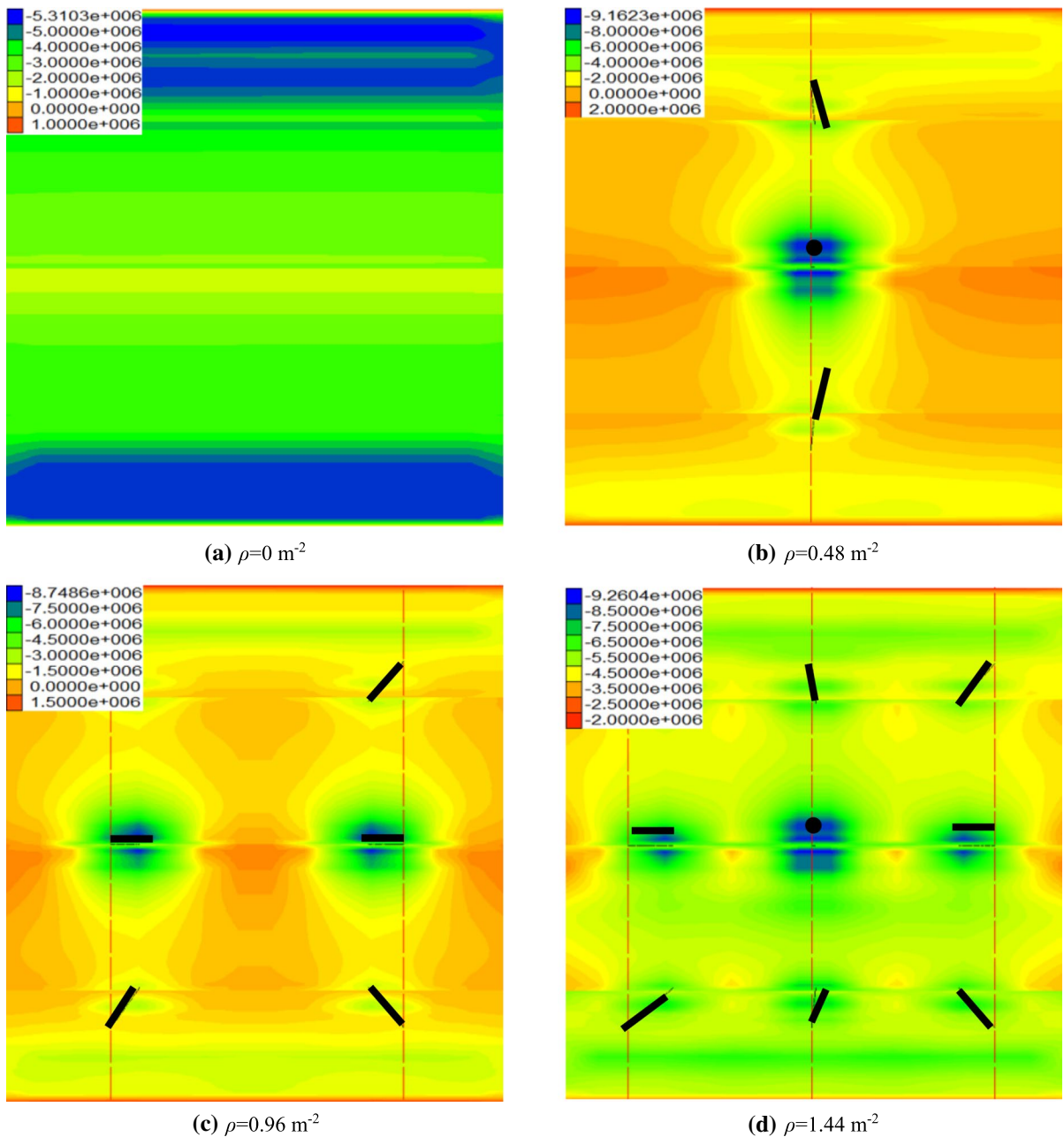


Fig. 11 Distribution of maximum principal stress inside jointed rock block of $\alpha=45^\circ$: **a** $\rho=0 \text{ m}^{-2}$; **b** $\rho=0.48 \text{ m}^{-2}$; $\rho=0.96 \text{ m}^{-2}$; $\rho=1.44 \text{ m}^{-2}$ (unit: Pa)

Moreover, we can also conclude from Fig. 11 that the formation of a compression zone near the bolt improved the resistance of the jointed rock blocks. After excavation of an underground tunnel, the original normal stress of the rock mass surface disappeared. It induced deformation and failure

toward the direction of the free surface. After applying anchor bolts, a circular stress compression zone formed around the bolt, which limited the further deformation and failure of the rock mass. Figure 11b–d, show that with the increase in bolt density, the compression zone overlapped with each other,

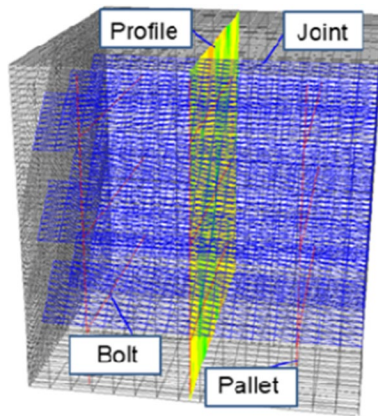


Fig. 12 Selected profile position in insides of jointed rock block

eventually compacting all of the joints into a state of compression.

To illustrate the support effect of anchor bolts under various joint dip angles, we chose another profile along the anchor bolt direction (see Fig. 12) to examine the stress distribution inside the rock blocks. Figure 13 displays the distribution of maximum principal stress inside jointed rock blocks with different joint dip angles. Note that images of maximum principal stress for jointed rock blocks with $\rho=0.00 \text{ m}^{-2}$ (i.e., with no bolts) and $\rho=1.44 \text{ m}^{-2}$ (with 9 bolts) were chosen for comparison of modeling results.

According to Fig. 13, for jointed rock blocks without bolts (i.e., $\rho=0.00 \text{ m}^{-2}$) with increasing joint dip angle from 0° to 90° , the stress concentration area was generally transferred from the rock bridges to the joint tips. For example, at $\alpha=0^\circ$, there was a high stress concentration in the rock bridge area near the middle joint, which was approximately 8.25 MPa, while near the joint tips, the stress value was only 2.0 MPa. With the increment of the joint dip angle, the stress concentration area was transferred to joint tips, while the stress value in the rock bridge area was reduced. In particular, at $\alpha=60^\circ$, a tensile stress of 0.17 MPa occurred. Moreover, with a further increase in the joint dip angle, the joints gradually became parallel to the loading direction, and the maximum principal stress in the middle of the rock bridge gradually increased due to the compression deformation of the rock mass toward the free surface. On the other hand, the principal stress at the joint tip decreased with the fracture failure of the rock blocks.

When the anchor bolts were applied, as shown in Fig. 13, the stress of the anchor bolt acting on the joints could be divided into compressive stress perpendicular to the joints and shear stress parallel along the joint inclination. The former formed the core of compressive stress in the nearby joints. With the increase in the joint dip angle, the core area first increased and then decreased. The core area of compressive stress reached the peak value at $\alpha=45^\circ$. The latter provided resistance for the rock to slide along the joint surface, and the appearance of the core zone of compressive stress on both sides of the joint reflected the anti-fracture efficiency of the bolt.

3.2 Influence of Anchor Bolts on Deformation

The maximum shear strain increment is one of the important parameters to reflect the degree of shear deformation of a rock mass. Thus, it is feasible and effective to study the failure state of the rock blocks and the support effect of the anchor bolt by means of the maximum cloud diagram of the shear strain increment of jointed rock blocks before and after anchorage. The distribution cloud map of the maximum shear strain increment in the jointed rock mass section before and after bolting is shown in Fig. 14.

As shown in Fig. 14, the joint dip angle dominated the tendentious failure pattern of the jointed rock blocks. When the joint dip angle was $0\text{--}30^\circ$, the parallel joint tips were interlinked, and the rock bridge showed the composite failure of tension and shear. When the joint dip angle was $45\text{--}60^\circ$, the shear failure tended to occur along the direction of joint inclination, forming a large controlled failure surface. In particular, at $\alpha=45^\circ$, only the middle set of nonpersistent joints was involved in the failure when no bolts were applied, which implied a tendentious path compared to others. When the joint dip angle was 75° , the failure at the lower left corner of the rock was more serious. The failure mode of the 90° joint dip model was similar to that of the rock block with no joints.

However, the application of anchor bolts resulted in the fracture of the jointed rock mass and increased the residual support strength. For instance, in Fig. 14a, the rock block was divided by the maximum shear strain increment cloud into three main parts, while after bolt support was applied, the divided part number was increased to ten, which means that the bolted rock block tended to be integral to resisting

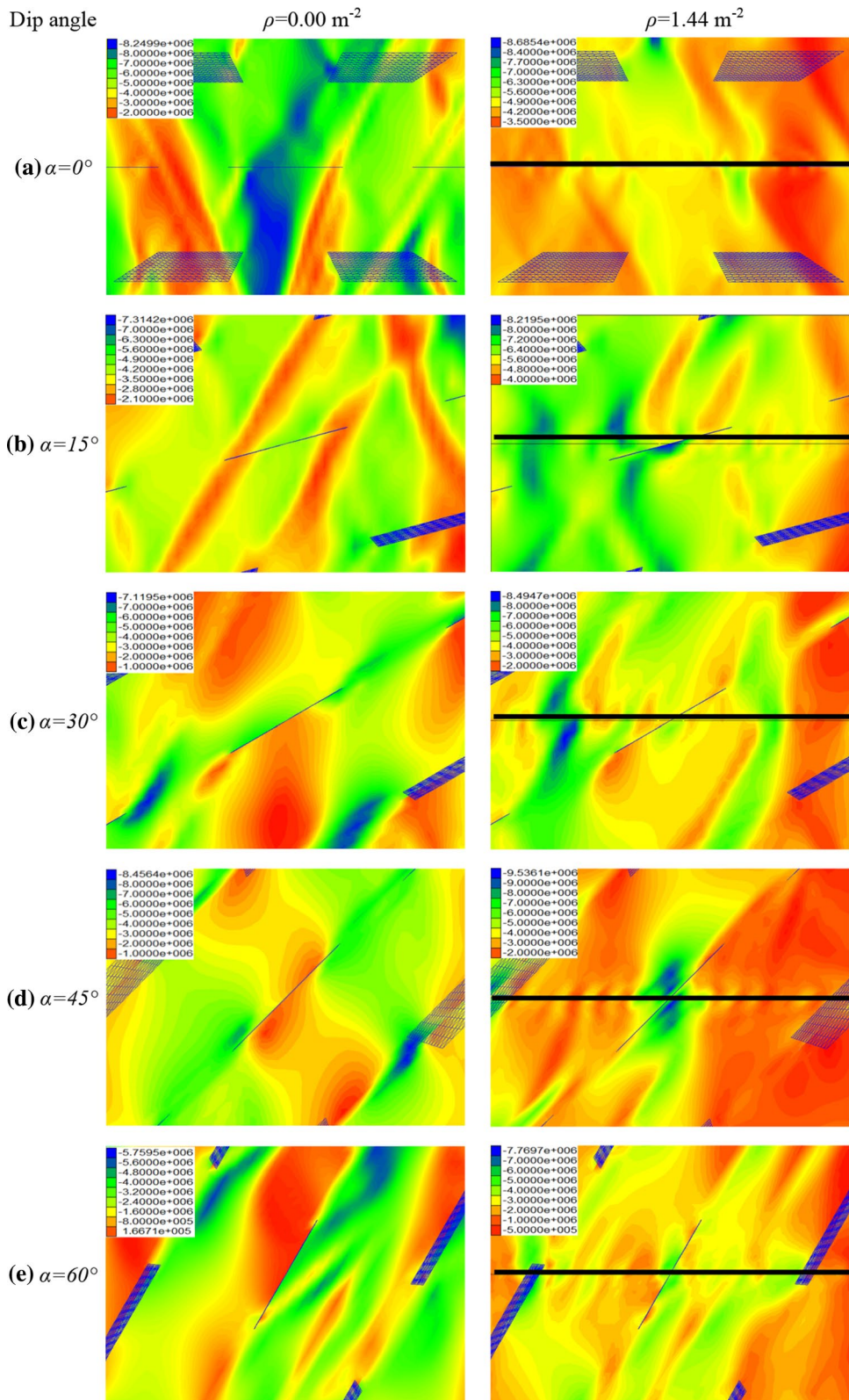


Fig. 13 Distribution of maximum principal stress inside jointed rock blocks under various joint orientations (unit: Pa)

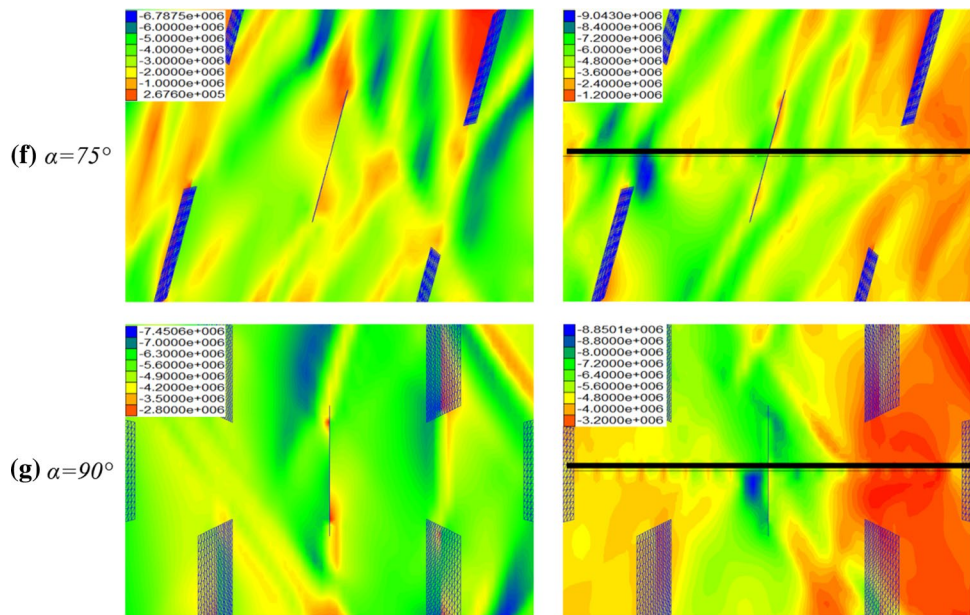


Fig. 13 (continued)

compression load. Under the compression loads, once the weak surface damage occurred in the rock blocks, the cohesive strength rapidly disappeared to enable the tendentious failure, and the departed block moved toward the free surface to lose bearing capacity. After applying bolts, the damaged rock blocks were still confined together by anchor bolts to continue carrying more compression loads.

4 Strength Performance of the Jointed Rock Blocks

The strength performance of the jointed rock blocks was always the focus on the support effect of the anchor bolts (Wu et al. 2017). Tables 3 and 4 list the peak strength and residual strength values of the jointed rock blocks with or without anchor bolts. Note that in Table 3, the values in the brackets for the joint dip angles of the 30° , 45° and 60° series imply the peak strength values obtained in the physical experiments. By comparing the peak strength between numerical modeling and physical experiments, it further demonstrated that the established numerical models were reasonable for investigating the support effect of anchor bolts on jointed rock blocks. From Tables 3 and 4, we can conclude that

the bolt number had a significant influence on the peak and residual strength of the jointed rock blocks but was dependent on the joint orientation. To better understand the influence of joint orientation on the strength performance of rock blocks, the relationship between strength values and joint dip angle was first investigated.

4.1 Influence of the Joint Dip Angle on the Strength Performance of the Rock Block Without Bolts

To study the influence of the joint dip angle on the strength of jointed rock blocks, the rock block strength values under different joint dip angles were normalized based on the strength of the intact rock block. In particular, Fig. 15 shows the variation in the normalized strength values of jointed rock blocks without anchor bolts.

As shown in Fig. 15, the peak strength of jointed rock blocks without bolts varied in a parabolic shape with the increase in joint dip angle from 0° to 90° with an interval of 15° . Specifically, when the joint angle was 0° , the peak strength was 85.1% of that for rock blocks with no joints. With α increasing to 15° and 30° , the normalized strength values decreased to 81.9% and 71.6%, respectively. This value arrived at the minimum at $\alpha = 45^\circ$, which was only 54.4% of the

Fig. 14 Distribution of the increment of maximum shear strain inside jointed rocks before and after bolting

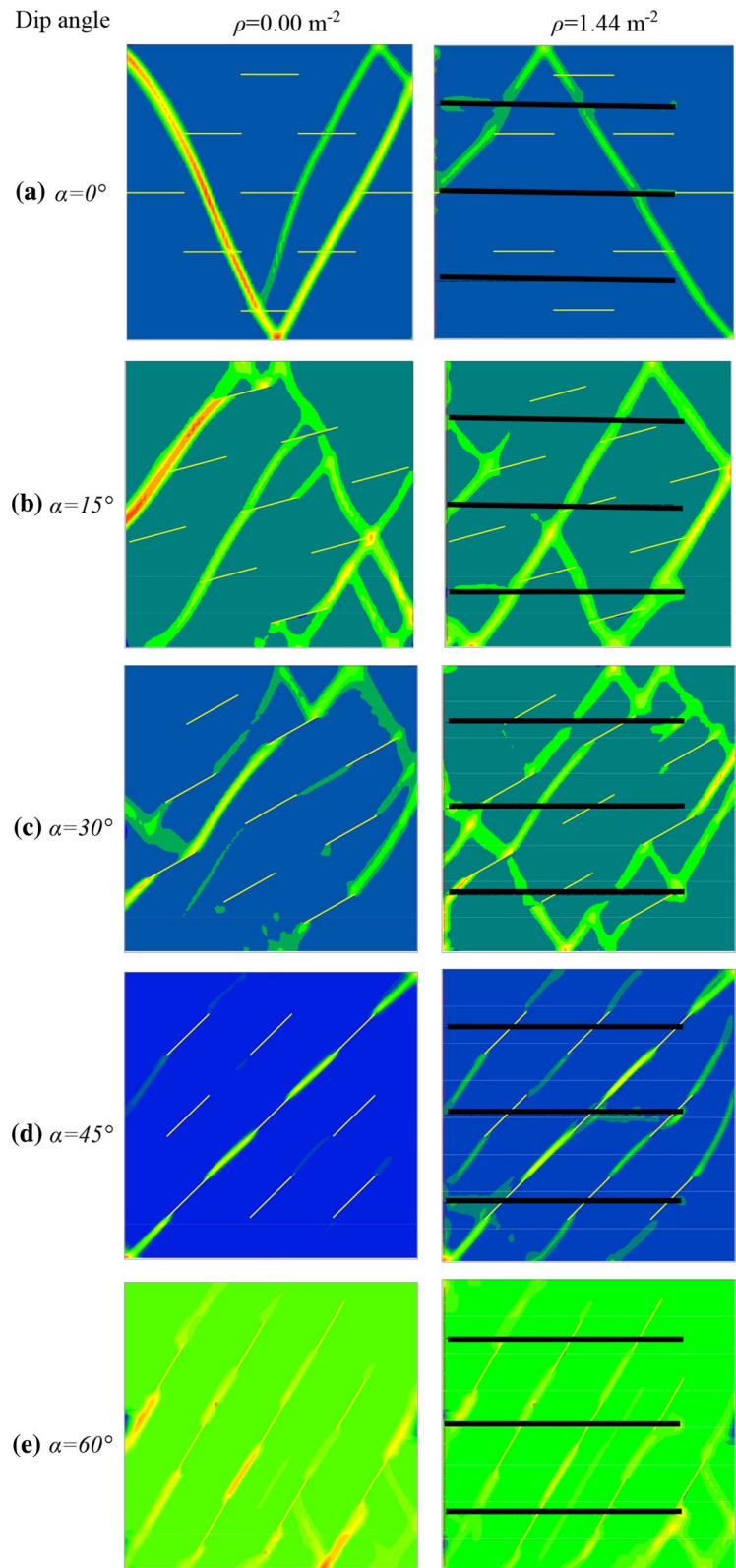


Fig. 14 (continued)

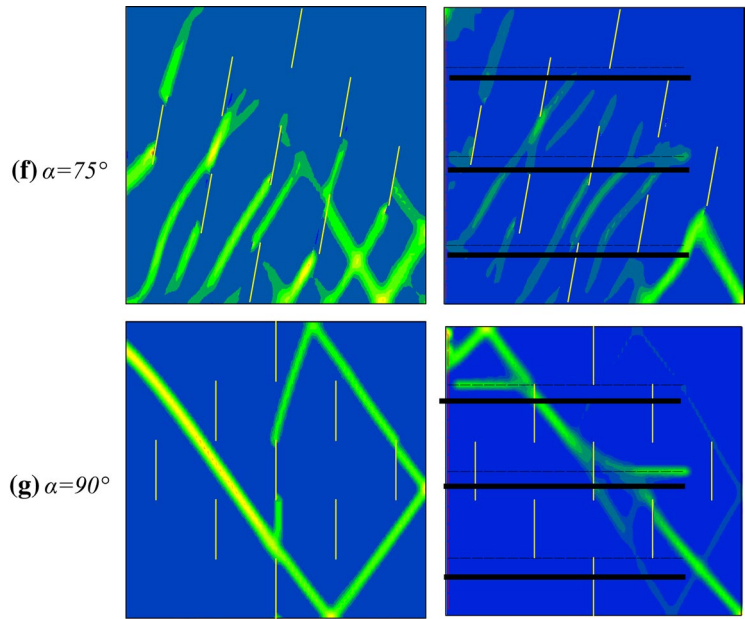


Table 3 Peak strength of jointed rock blocks with or without anchored bolts

Joint dip angle, α /deg	Bolt density (m^{-2})			
	0	0.48	0.96	1.44
No joints	5.25	5.69	6.21	7.99
0	4.47	4.78	5.16	6.65
15	4.30	4.66	5.07	6.55
30	3.76 (3.69)	4.09 (3.94)	4.45 (4.41)	5.79 (6.06)
45	2.86 (2.52)	3.22 (2.78)	3.60 (4.07)	4.94 (4.56)
60	3.07 (2.28)	3.35 (4.20)	3.70 (4.28)	5.14 (5.20)
75	4.37	4.80	5.25	6.78
90	5.07	5.47	5.96	7.69

Table 4 Residual strength of jointed rock blocks with or without anchored bolts

Joint dip angle, α /deg	Bolt density (m^{-2})			
	0	0.48	0.96	1.44
No joints	2.462	2.979	3.578	5.224
0	2.423	2.952	3.368	4.769
15	2.424	2.932	3.514	5.100
30	2.111	2.766	3.323	4.890
45	1.572	2.319	2.911	4.663
60	1.924	2.600	3.185	4.840
75	2.348	2.913	3.557	5.179
90	2.427	2.945	3.568	4.600

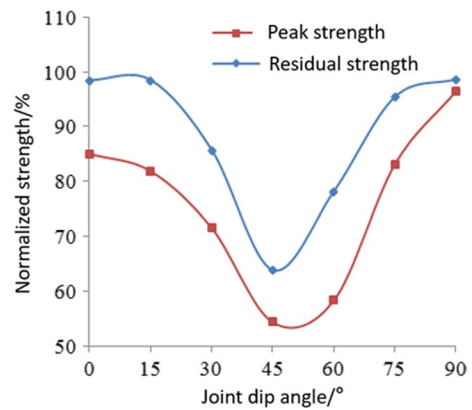


Fig. 15 Variation of normalized strength values of unbolted rock blocks with joint dip angle

rock blocks with no joints. Afterward, the normalized peak strength gradually increased; when the dip angle was 90° , the value was 96.5%, which means that the peak strength was negligibly affected by joints.

Moreover, the relationship between residual strength and the joint dip angle was similar to that between peak strength and joint dip angle. However, when the joint dip angle was 0° – 15° or 75° – 90° , the normalized residual strength values were between 95.4–98.6%, while for the rest of the joint dip angles, the normalized residual strengths were 63.8–85.7%. Compared with the peak strength, the residual

strength of the jointed rock blocks was larger than that of the peak strength, indicating that the joints had less influence on the residual strength of the rock blocks than on the peak strength.

4.2 Influence of Bolt Density on the Strength Performance of Rock Blocks

In view of the significance of the joint dip angle on the strength performance of rock blocks, the influence of the bolt density was analyzed under various joint dip angles. Figure 16 displays the variations in the peak strength and residual strength values of jointed rock blocks with bolt density under different joint dip angles.

The peak strength and residual strength of the jointed rock blocks had a cubic function relation with the joint dip angle or bolt density. With the increase in the joint dip angle, the rock block strength first decreased and then increased with a minimum value at $\alpha=45^\circ$ regardless of the bolt density. The three-dimensional functional diagram of peak strength with joint dip angle and bolt density showed an inverted "tile" shape, while the three-dimensional functional diagram of residual strength with joint dip angle and bolt density showed a "scallop" shape. The change in the joint dip angle had a weaker influence on the

residual strength than on the peak strength under various bolt densities.

To further demonstrate the supporting effect of anchorage on jointed rock blocks, the rock block strength under different joint orientations without bolts was utilized to normalize the strength increments of rock blocks when different densities of bolts were applied. Figure 17 displays the variation in the strength increment ratios of rock blocks with bolt density.

As shown in Fig. 17a, with increasing bolt density, the increment ratios of the peak strength of the jointed rock blocks also increased rapidly. When the joint dip angle was 45° , the maximum increment of the peak strength of the jointed rock block was achieved under the same bolt density. Moreover, the variation in the residual strength increment ratios with the bolt density was similar to that for the peak strength increment. The maximum increment of the residual strength of the jointed rock block was also achieved at $\alpha=45^\circ$, which was 2.97 when the applied bolt density was 1.44 m^{-2} . A further comparison between Figs. 17a, b shows that the increments of residual strength were always larger than those of peak strength regardless of the bolt density, which demonstrated that the most important role of bolt support was to improve the postpeak strength of the rock mass to maintain stability after rock mass failure.

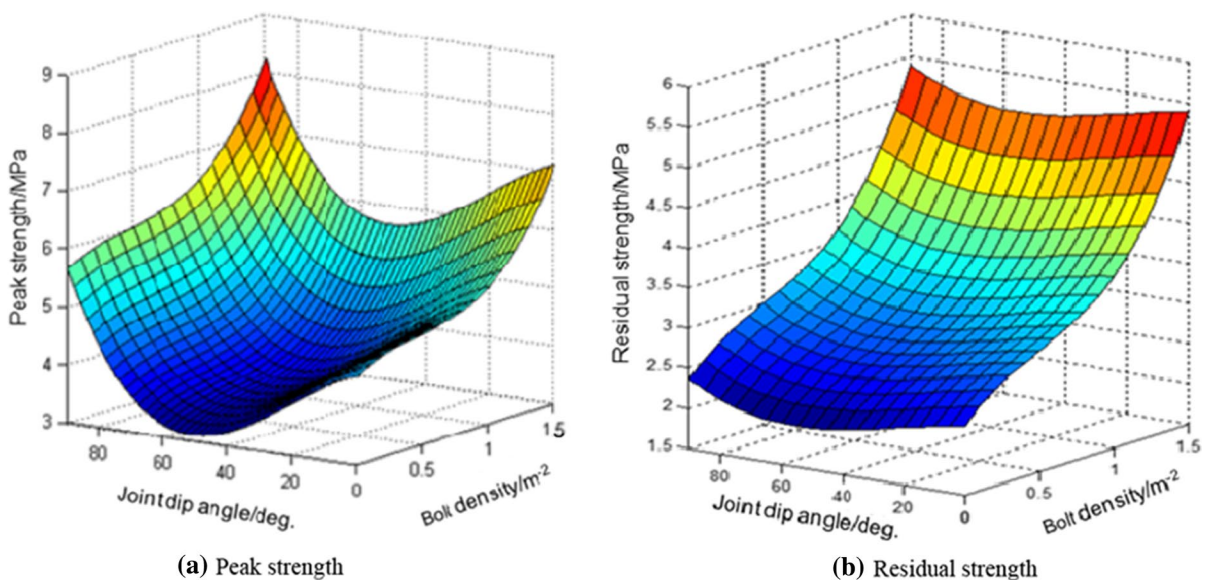
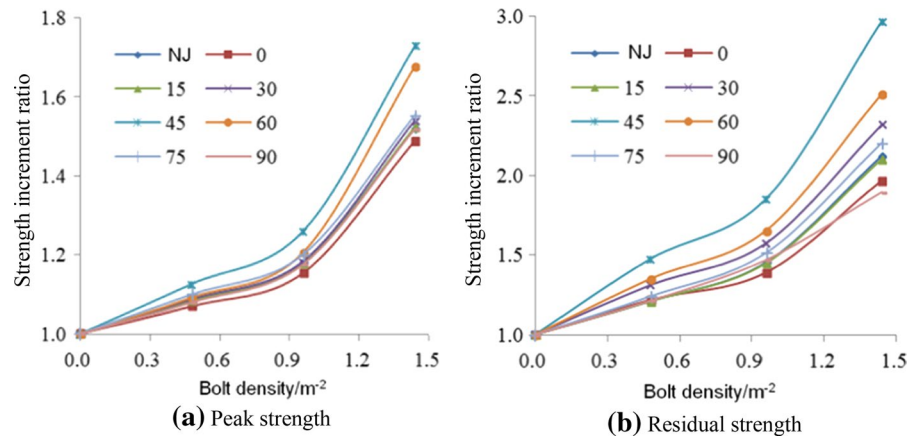


Fig. 16 Variation of strength values of rock blocks with bolt density: **a** peak strength; **b** residual strength

Fig. 17 Variation of strength increment times of rock blocks with bolt density: **a** peak strength; **b** residual strength



Even though we significantly improved the resistance capability of the jointed rock blocks by incorporating anchor bolts in accordance with Fig. 17, it was noteworthy that the strength for some bolted jointed rock blocks was still less than that for intact rock blocks (i.e., without joints), as shown in Tables 3 and 4. Thus, the unified design of the anchor bolt support scheme might account for the failure of bolted rock masses in underground projects. The orientation of the incipient joints should be taken into consideration for support design.

5 Conclusions

A series of numerical modeling experiments have been carried out in the present study to examine the support effect of anchor bolts on rock blocks containing incipient joints. The setup of the numerical models strictly followed the physical experiments conducted in the laboratory and was validated by the experimental results. By conducting compression tests on the jointed rock models, the major findings can be drawn as follows.

1. A novel method has been proposed to establish rock block models containing incipient joints. The comparison of test results between numerical simulations and physical experiments indicates that the numerical models were well established to derive the mechanical behaviors of jointed rock blocks adjacent to underground tunnels.
2. With increasing bolt density, the increment ratios of the peak strength of the jointed rock blocks

also increase rapidly, and the greater the bolt density is, the greater the increment. When the joint dip angle was 45°, the maximum increment of the peak strength of the jointed rock block was achieved under the same bolt density.

3. The application of an anchor bolt reduces the nonuniformity of the stress distribution in jointed rock blocks, and the uniformity increases gradually with increasing bolt density. The formation of a compression zone induced by the anchor bolts improves the resistance of the jointed rock blocks.
4. The rock blocks containing incipient joints have different tendentious failure patterns that are dependent on joint orientation. By applying anchor bolts, the tendentious failure pattern would be contained, especially at $\alpha=45^\circ$, for which a core of compressive stress would reduce the shearing failure along the joints plane.

Acknowledgements This research was supported by the National Natural Science Foundation of China (Grant Nos. 51734009 and 51704183) and Postdoctoral Science Foundation of China (Grant No. 2018M640646).

Funding The authors have not disclosed any funding.

Data Availability Enquiries about data availability should be directed to the authors.

Declarations

Conflict of Interest The authors declare no conflict of interest.

References

- Cao RH, Cao P, Lin H, Ma GW, Zhang CY, Jiang C (2018) Failure characteristics of jointed rock-like material containing multi-joints under a compressive-shear test: experimental and numerical analyses. *Int J Arch Civ Mech Eng* 18(3):784–798
- Cao RH, Lin H, Lin Q, Meng J (2020) Failure mechanism of non-persistent jointed rock-like specimens under uniaxial loading: laboratory testing. *Int J Rock Mech Min Sci* 132:104341
- Grasselli G (2005) 3D Behaviour of bolted rock joints: experimental and numerical study. *Int J Rock Mech Min Sci* 42:13–24
- Haas CJ (1981) Analysis of rock bolting to prevent shear movement in fractured ground. *Int J Rock Mech Min Sci* 33:698–704
- Han GS, Jing HW, Jiang YJ et al (2018) The effect of joint dip angle on the mechanical behavior of infilled jointed rock masses under uniaxial and biaxial compressions. *Processes* 6(5):49
- Hencher RS (2014) Characterizing discontinuities in naturally fractured outcrop analogues and rock core: the need to consider fracture development over geological time. *Geol Soc Lond Spec Publ* 374(1):113–123
- Indraratna B, Aziz NI, Dey A (2001) Behaviour of joints containing clay infill under constant normal stiffness, with and without bolting. *Geotechn Eng* 149(4):259–267
- Jing HW, Yang SQ, Zhang ML et al (2014) An experimental study on anchorage strength and deformation behavior of large-scale jointed rock mass. *Tunn Undergr Space Techn* 43:184–197
- Lajtai EZ, Carter BJ, Duncan E (1994) En echelon crack-arrays in potash salt rock. *Rock Mech Rock Eng* 27(2):89–111
- Li SC, Wang G, Wang SG et al (2006) Application of fracture-damage model to anchorage of discontinuous jointed rock mass of excavation and supporting. *Chin J Rock Mech Eng* 25(8):1582–1590
- Li SJ, Feng XT, Li Z et al (2012) In situ monitoring of rock burst nucleation and evolution in the deeply buried tunnels of Jinping II hydropower station. *Eng Geol* 137–138:85–96
- Meng B, Jing HW, Yang XX, Chen KF, Yang SQ (2013) Experimental study of deformation and failure characteristics of anchorage unit in fractured surrounding rocks. *Chin J Rock Mech Eng* 32(12):2497–2505
- Pellet F, Egger P (1996) Analytical model for the mechanical behavior of bolted rock joints subjected to shearing. *Rock Mech Rock Eng* 29:73–97
- Sun PP, Yang XX, Sun DK, Qiao WG, Wu Y (2019) Geometric and mechanical properties of a shear-formed fracture occurring in a rock bridge between discontinuous joints. *Bull Eng Geol Environm* 79:1365–1380
- Wang G, Zhang YZ, Jiang YJ et al (2018) Shear behaviour and acoustic emission characteristics of bolted rock joints with different roughnesses. *Rock Mech Rock Eng* 51:1885–1906
- Wong RHC, Chau KT (1998) Crack coalescence in a rock-like material containing two cracks. *Int J Rock Mech Min Sci* 35:147–164
- Wong RHC, Chau KT, Tang CA, Lin P (2001) Analysis of crack coalescence in rock-like materials containing three flaws-part I: experimental approach. *Int J Rock Mech Min Sci* 38:909–924
- Wu XZ, Jiang YJ, Li B (2017) Influence of joint roughness on the shear behaviour of fully encapsulated rock bolt. *Rock Mech Rock Eng* 51:953–959
- Yang XX, Kulatilake P (2019) Laboratory investigation of mechanical behavior of granite samples containing discontinuous joints through direct shear tests. *Arab J Geosci* 12(2):79
- Yang XX, Qiao WG (2018) Numerical investigation of the shear behavior of granite materials containing discontinuous joints by utilizing the flat-joint model. *Comput Geotech* 104:69–80
- Yang XX, Kulatilake P, Jing HW, Yang SQ (2015) Numerical simulation of a jointed rock block mechanical behavior adjacent to an underground excavation and comparison with physical model test results. *Tunn Undergr Space Techn* 50:129–142
- Yang XX, Jing HW, Tang CA, Yang SQ (2017) Effect of parallel joint interaction on mechanical behavior of jointed rock mass models. *Int J Rock Mech Min Sci* 92:40–53
- Zhang ML (2013) Research on crack evolution and bolting mechanism of intermittently jointed rocks. China University of Mining and Technology, Xuzhou

Publisher's Note Springer Nature remains neutral with regard to jurisdictional claims in published maps and institutional affiliations.

Springer Nature or its licensor holds exclusive rights to this article under a publishing agreement with the author(s) or other rightsholder(s); author self-archiving of the accepted manuscript version of this article is solely governed by the terms of such publishing agreement and applicable law.